Nuclear Engineering and Technology 51 (2019) 1504–1513

Contents lists available at ScienceDirect

Nuclear Engineering and Technology

journal homepage: www.elsevier.com/locate/net

Original Article

Two-fluid equations for two-phase flows in moving systems

Byoung Jae Kim [a, *], Myung Ho Kim [a], Seung Wook Lee [b], Kyung Doo Kim [b, **]

[a] School of Mechanical Engineering, Chungnam National University, 99 Daehak-ro, Yuseong-gu, Daejeon, 34134, Republic of Korea
[b] Thermal-Hydraulic Safety Research Division, Korea Atomic Energy Research Institute, 111 Daedeok-daero 989, Yuseong-gu, Daejeon, 305-353, Republic of Korea

ARTICLE INFO

Article history:
Received 6 February 2019
Received in revised form
5 April 2019
Accepted 30 April 2019
Available online 1 May 2019

Keywords:
Ocean nuclear reactor
Thermal-hydraulics
Two-fluid equation
Moving system

ABSTRACT

Recently, ocean nuclear reactors have received attention due to enhanced safety features. The movable and transportable characteristics distinguish ocean nuclear reactors from land-based nuclear reactors. Therefore, for safety/design analysis of the ocean reactor, the thermos-hydraulics must be investigated in the moving system. However, there are no studies reporting the general two-fluid equations that can be used for multi-dimensional simulations of two-phase flows in moving systems. This study is to systematically formulate the multi-dimensional two-fluid equations in the non-inertial frame of reference. To demonstrate the applicability of the formulated equations, we perform a total of six different simulations in 2D tanks with translational and/or rotational motions.
© 2019 Korean Nuclear Society, Published by Elsevier Korea LLC. This is an open access article under the CC BY-NC-ND license (http://creativecommons.org/licenses/by-nc-nd/4.0/).

1. Introduction

Recently, various concepts have been proposed for ocean nuclear power plants with enhanced safety features [1–3]. The ocean nuclear reactor is characterized by the motion of the reactor system according to ocean environments. They are transportable and moveable, and thus the thermal-hydraulic behavior must be investigated in the moving systems.

There are two numerical approaches to predict the thermal-hydraulic behavior in the moving systems. One is the one-fluid approach with an interface tracking techniques. This one-fluid approach has been widely used for the liquefied natural gas cargos in the ship industry [4–9]. However, existing studies were limited to flows with large interfaces. Though this approach does not require a parameter tuning process, it is not practical for two-phase flows in nuclear systems. The other is the two-fluid approach. The two-fluid model has been widely used for practical applications involving two-phase flows in nuclear reactors. Though the accuracy depends on various modeling terms, the two-fluid model can yield satisfactory results for flows with both small and large interfaces in a large flow domain.

The existing two-fluid equations are obtained by applying the time-, volume-, or ensemble-averaging method to the mass, momentum, and energy conservation equations in the absolute frame of reference [10–12]. To predict two-phase flows inside floating or submerged platforms, the two-fluid equations must be modified to account for the effects of arbitrary motions of the nuclear systems. Some previous works utilized the one-dimensional two-fluid equations with the aim of system analysis in oscillating conditions [13–18]. However, the one-dimensional simulation inherently loses multi-dimensional flow characteristics.

To the best of our knowledge, there are no studies on multi-dimensional simulations based on the two-fluid model in a moving system. This paper suggests the two-fluid equations in the non-inertial frame of reference. Six different simulations in 2D tanks with translational and/or rotational motions demonstrate the applicability of the two-fluid model to two-phase flows with both large and small interfaces in moving systems.

2. Single-phase flow

Fig. 1 shows two different frames of reference. The absolute frame is expressed in terms of the Cartesian coordinates (X, Y, Z). The moving frame is undergoing acceleration with respect to the absolute frame and is expressed in terms of the Cartesian coordinates (x, y, z). The moving frame is located by position vector $\mathbf{R}$ relative to the absolute frame and rotates with an angular velocity vector of $\mathbf{\Omega}$. A particle is instantaneously located with respect to the moving frame by position vector $\mathbf{r}$.

While the conservation equations for the thermodynamic properties remain formally unchanged under a change of frame, the

* Corresponding author.
** Corresponding author.
E-mail addresses: bjkim@cnu.ac.kr (B.J. Kim), kdkim@kaeri.re.kr (K.D. Kim).

https://doi.org/10.1016/j.net.2019.04.022
1738-5733/© 2019 Korean Nuclear Society, Published by Elsevier Korea LLC. This is an open access article under the CC BY-NC-ND license (http://creativecommons.org/licenses/by-nc-nd/4.0/).

Nomenclature

f	Force vector, N/m^3
g	Gravitational acceleration vector, m^2/s
p	Pressure, Pa
r	Position vector with respect to the moving frame of reference, m
u	Fluid velocity vector, m/s
I	3 × 3 identity matrix
M	Force vector, N/m^3
R	Position vector relative to the absolute frame of reference, m
V	Volume, m^3

Greeks

α	Phase fraction
λ	Fluid bulk viscosity, Pa · s
μ	Fluid dynamic viscosity, Pa · s
ρ	Fluid density, kg/m^3
$\boldsymbol{\tau}$	Viscous stress tensor
$\boldsymbol{\Omega}$	Rotation vector

Superscript

Re	Reynolds stress

Subscripts

k	Phase indicator
g	Gas phase
l	Liquid phase
ki	k phase at the interface
ik	k phase at the interface

Symbols

$=$	Phase mean value
$\hat{}$	Mass-weighted mean value
$\dot{}$	Frist time derivative (d/dt)
$\ddot{}$	Second time derivative (d^2/dt^2)

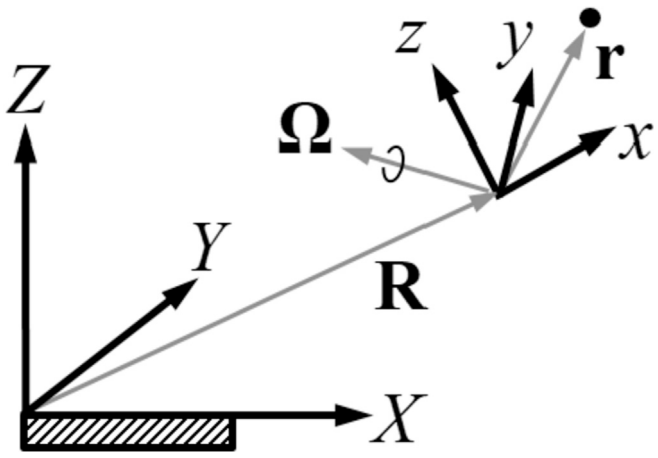

Fig. 1. Two frames of reference.

local instantaneous equation for momentum is expressed as follows:

$$\rho\frac{D\mathbf{u}}{Dt} = -\nabla p + \nabla\cdot\left[\mu\left(\nabla\mathbf{u} + (\nabla\mathbf{u})^T\right) + \lambda(\nabla\cdot\mathbf{u})\mathbf{I}\right] + \rho\mathbf{g} + \mathbf{f}_{\text{interial}}, \quad (1)$$

$\mathbf{f}_{\text{interial}}$ includes four effects. The first term on the right-hand side of Eq. (2) accounts for the translational acceleration of the moving frame with respect to the absolute frame ($\ddot{\mathbf{R}} = d^2\mathbf{R}/dt^2$). The last three terms in Eq. (2) are the Euler force for spin-up or spin-down ($\dot{\boldsymbol{\Omega}} = d\boldsymbol{\Omega}/dt$), the Coriolis force, and the centripetal force, respectively, which arise from the rotation of the moving frame with respect to the absolute frame. The position vector **r** in Eq. (2) is replaced by the distance vector from the rotational axis to the local position in the moving frame.

3. Two-phase flow

3.1. Volume-averaged equations

The local instantaneous conservation equation for mass remains formally unchanged under a change of frame. Thus, the averaged mass equation for a two-phase flow in the moving frame is identical to that in the absolute frame. The same is true for the internal energy and enthalpy. The averaged equation forms for internal energy and enthalpy are invariant under a change of frame.

However, the form of the averaged momentum equation in the moving frame would differ from that in the absolute frame due to the presence of the additional term $\mathbf{f}_{\text{interial}}$ given by Eq. (2). Drew [10] rigorously derived the volume-averaged two-fluid equations in the absolute frame. Here, we consider the adiabatic two-phase flow. The volume-averaged momentum equation for phase k in the absolute frame is given by

$$\frac{\partial}{\partial t}\left(\alpha_k\bar{\bar{\rho}}_k\widehat{\mathbf{u}_k}\right) + \nabla\cdot\left(\alpha_k\bar{\bar{\rho}}_k\widehat{\mathbf{u}_k}\widehat{\mathbf{u}_k}\right) = -\alpha_k\nabla\bar{\bar{p}}_k + \nabla\cdot\left[\alpha_k\left(\bar{\bar{\boldsymbol{\tau}}}_k + \boldsymbol{\tau}_k^{\text{Re}}\right)\right] + \alpha_k\bar{\bar{\rho}}_k\mathbf{g} + (\bar{\bar{p}}_{ki} - \bar{\bar{p}}_k)\nabla\alpha_k + \mathbf{M}_{ik} - \nabla\alpha_k\cdot\bar{\bar{\boldsymbol{\tau}}}_{ki}, \quad (3)$$

$$\mathbf{f}_{\text{interial}} = -\rho\ddot{\mathbf{R}} - \rho\dot{\boldsymbol{\Omega}}\times\mathbf{r} - 2\rho\boldsymbol{\Omega}\times\mathbf{u} - \rho\boldsymbol{\Omega}\times(\boldsymbol{\Omega}\times\mathbf{r}), \quad (2)$$

where ρ, **u**, p, μ, λ, **I**, and **g** are the density, the velocity vector, the pressure, the viscosity, the bulk viscosity, the identity matrix, and the gravitational acceleration, respectively. The additional term

where the double over-bar ($=$) and the over-hat ($\hat{}$) indicate the phase mean and mass-weighted mean, respectively (Appendix A). In the above equation, α_k, $\boldsymbol{\tau}_k$, $\boldsymbol{\tau}_k^{\text{Re}}$, p_{ki}, $\mathbf{M}_{ik}$, and $\boldsymbol{\tau}_{ki}$ are the void fraction, the viscous stress tensor, the Reynolds stress tensor, the fluid pressure at the interface, the interfacial momentum transfer,

and the fluid viscous stress tensor at the interface, respectively.

We now consider the local instantaneous momentum equation for phase k in the moving frame as

$$\rho_k \frac{D\mathbf{u}_k}{Dt} = -\nabla p_k + \nabla \cdot \left[\mu_k\left(\nabla \mathbf{u}_k + (\nabla \mathbf{u}_k)^T\right) + \lambda_k(\nabla \cdot \mathbf{u}_k)\mathbf{I}\right] + \rho_k \mathbf{g} + \mathbf{f}_{\text{interial},k}, \tag{4}$$

$$\mathbf{f}_{\text{interial},k} = -\rho_k \ddot{\mathbf{R}} - \rho_k \dot{\boldsymbol{\Omega}} \times \mathbf{r}_k - 2\rho_k \boldsymbol{\Omega} \times \mathbf{u}_k - \rho_k \boldsymbol{\Omega} \times (\boldsymbol{\Omega} \times \mathbf{r}_k). \tag{5}$$

The volume averaging over Eq. (4) without $\mathbf{f}_{\text{interial},k}$ leads to Eq. (3). Hence, we just have to concentrate on $\mathbf{f}_{\text{interial},k}$. Taking the volume average over $\mathbf{f}_{\text{interial},k}$,

$$\begin{aligned}\mathbf{F}_{\text{interial},k} &= \frac{1}{V}\int_{V_k} \mathbf{f}_{\text{interial},k} dV \\ &= -\frac{1}{V}\int_{V_k} \rho_k \ddot{\mathbf{R}} dV - \frac{1}{V}\int_{V_k} \rho_k \dot{\boldsymbol{\Omega}} \times \mathbf{r}_k dV - \frac{1}{V}\int_{V_k} 2\rho_k \boldsymbol{\Omega} \times \mathbf{u}_k dV - \frac{1}{V}\int_{V_k} \rho_k \boldsymbol{\Omega} \times (\boldsymbol{\Omega} \times \mathbf{r}_k) dV,\end{aligned} \tag{6}$$

where V and V_k are the total averaging volume and the sub-volume occupied by phase k, respectively. $\mathbf{R}$ and $\boldsymbol{\Omega}$ are functions of time alone, being independent of the local position. Using the phase and mass-weighted means, one can write each term on the right-hand side of Eq. (6) as follows:

$$-\frac{1}{V}\int_{V_k} \rho_k \ddot{\mathbf{R}} dV = \left(-\frac{1}{V}\int_{V_k} \rho_k dV\right)\ddot{\mathbf{R}} = -\alpha_k \bar{\bar{\rho}}_k \ddot{\mathbf{R}}, \tag{7}$$

$$\begin{aligned}-\frac{1}{V}\int_{V_k} \rho_k \dot{\boldsymbol{\Omega}} \times \mathbf{r}_k dV &= -\dot{\boldsymbol{\Omega}} \times \left(\frac{1}{V}\int_{V_k} \rho_k \mathbf{r}_k dV\right) = -\dot{\boldsymbol{\Omega}} \times \left(\alpha_k \bar{\bar{\rho}}_k \widehat{\mathbf{r}_k}\right) \\ &= -\alpha_k \bar{\bar{\rho}}_k \dot{\boldsymbol{\Omega}} \times \widehat{\mathbf{r}_k},\end{aligned} \tag{8}$$

$$\begin{aligned}-\frac{1}{V}\int_{V_k} 2\rho_k \boldsymbol{\Omega} \times \mathbf{u}_k dV &= -2\boldsymbol{\Omega} \times \left(\frac{1}{V}\int_{V_k} \rho_k \mathbf{u}_k dV\right) \\ &= -2\boldsymbol{\Omega} \times \left(\alpha_k \bar{\bar{\rho}}_k \widehat{\mathbf{u}_k}\right) = -2\alpha_k \bar{\bar{\rho}}_k \boldsymbol{\Omega} \times \widehat{\mathbf{u}_k},\end{aligned} \tag{9}$$

$$\begin{aligned}-\frac{1}{V}\int_{V_k} \rho_k \boldsymbol{\Omega} \times (\boldsymbol{\Omega} \times \mathbf{r}_k) dV &= -\boldsymbol{\Omega} \times \left[\boldsymbol{\Omega} \times \left(\frac{1}{V}\int_{V_k} \rho_k \mathbf{r}_k dV\right)\right] \\ &= -\boldsymbol{\Omega} \times \left[\boldsymbol{\Omega} \times \left(\alpha_k \bar{\bar{\rho}}_k \widehat{\mathbf{r}_k}\right)\right] \\ &= -\alpha_k \bar{\bar{\rho}}_k \boldsymbol{\Omega} \times \left(\boldsymbol{\Omega} \times \widehat{\mathbf{r}_k}\right).\end{aligned} \tag{10}$$

Combining Eq. (7)~(10), we obtain

$$\begin{aligned}\mathbf{F}_{\text{interial},k} = &-\alpha_k \bar{\bar{\rho}}_k \ddot{\mathbf{R}} - \alpha_k \bar{\bar{\rho}}_k \dot{\boldsymbol{\Omega}} \times \widehat{\mathbf{r}_k} - 2\alpha_k \bar{\bar{\rho}}_k \boldsymbol{\Omega} \times \widehat{\mathbf{u}_k} - \alpha_k \bar{\bar{\rho}}_k \boldsymbol{\Omega} \\ &\times \left(\boldsymbol{\Omega} \times \widehat{\mathbf{r}_k}\right).\end{aligned} \tag{11}$$

Equation (11) consists of the translational acceleration effect, the Euler force for spin-up or spin-down, the Coriolis force, and the centripetal force. It is interesting to note that the variables are not coupled in Eq. (11), which is desirable in view of the numerical simulation. $\widehat{\mathbf{r}_k} = \overline{\overline{\rho_k \mathbf{r}_k}}/\bar{\bar{\rho}}_k$ can be interpreted as the center-of-mass for phase k within the total averaging volume. If the flow is incompressible, $\widehat{\mathbf{r}_k} = \bar{\bar{\mathbf{r}}}_k$ is the center-of-geometry for phase k within the total averaging volume. If the flow is a uniformly distributed incompressible bubbly flow, $\widehat{\mathbf{r}_k}$ becomes the center-of-geometry of the total averaging volume.

The volume-averaged momentum equation in the moving frame is obtained by adding Eq. (11) to the existing form of the volume-averaged momentum equation in the absolute frame. The resultant equation is

$$\frac{\partial}{\partial t}\left(\alpha_k\bar{\bar{\rho}}_k\widehat{\mathbf{u}_k}\right)+\nabla\cdot\left(\alpha_k\bar{\bar{\rho}}_k\widehat{\mathbf{u}_k}\widehat{\mathbf{u}_k}\right)=-\alpha_k\nabla\bar{\bar{p}}_k+\nabla\cdot\left[\alpha_k\left(\bar{\bar{\tau}}_k+\tau_k^{\mathrm{Re}}\right)\right]+\alpha_k\bar{\bar{\rho}}_k\mathbf{g}$$
$$+(\bar{\bar{p}}_{ki}-\bar{\bar{p}}_k)\nabla\alpha_k+\widehat{\mathbf{u}_{ki}}\Gamma_k+\mathbf{M}_{ik}-\nabla\alpha_k\cdot\bar{\bar{\tau}}_{ki}$$
$$-\alpha_k\bar{\bar{\rho}}_k\ddot{\mathbf{R}}-\alpha_k\bar{\bar{\rho}}_k\dot{\mathbf{\Omega}}\times\widehat{\mathbf{r}_k}-2\alpha_k\bar{\bar{\rho}}_k\mathbf{\Omega}\times\widehat{\mathbf{u}_k}-\alpha_k\bar{\bar{\rho}}_k\mathbf{\Omega}\times\left(\mathbf{\Omega}\times\widehat{\mathbf{r}_k}\right) \quad (12)$$

All variables in Eq. (12) are to be measured in the moving frame.

3.2. Time-averaged equations

We now turn to the time-averaged momentum equation. Time-averaging is performed at a fixed local point in the moving frame. The time average of the momentum equation in the absolute frame is well known [11,19]. Thus, we concentrate on the additional term given by Eq. (2). $\mathbf{\Omega}$ and $\mathbf{R}$ are continuous functions of time, and the local point is alternatively occupied by gas and liquid. Accordingly, one can write the local instantaneous additional term for phase k as

$$\mathbf{f}_{\mathrm{interial},k}=-\rho_k\ddot{\mathbf{R}}-\rho_k\dot{\mathbf{\Omega}}\times\mathbf{r}-2\rho_k\mathbf{\Omega}\times\mathbf{u}_k-\rho_k\mathbf{\Omega}\times(\mathbf{\Omega}\times\mathbf{r}). \quad (13)$$

The existing time-averaged conservation equations have interfacial transfer terms resulting from the time average of the spatial or time derivatives in the local instantaneous conservation equations [19]. However, Eq. (13) does not have spatial or time derivatives. Hence, the time average of Eq. (13) does not yield interfacial momentum transfer terms.

Taking the time average of Eq. (13),

$$\mathbf{F}_{\mathrm{interial},k}=\frac{1}{\Delta t}\int_{[\Delta t]_k}\mathbf{f}_{\mathrm{interial},k}dt$$
$$=-\frac{1}{\Delta t}\int_{[\Delta t]_k}\rho_k\ddot{\mathbf{R}}dt-\frac{1}{\Delta t}\int_{[\Delta t]_k}\rho_k\dot{\mathbf{\Omega}}\times\mathbf{r}dt-\frac{1}{\Delta t}\int_{[\Delta t]_k}2\rho_k\mathbf{\Omega}\times\mathbf{u}_kdt-\frac{1}{\Delta t}\int_{[\Delta t]_k}\rho_k\mathbf{\Omega}\times(\mathbf{\Omega}\times\mathbf{r})dt, \quad (14)$$

where Δt is the time interval of the averaging, and $[\Delta t]_k$ is part of Δt in which the local point is occupied by phase k. Using the phase and mass-weighted means, one can write each term on the right-hand side of Eq. (14) as follows:

$$-\frac{1}{\Delta t}\int_{[\Delta t]_k}\rho_k\ddot{\mathbf{R}}dt=-\alpha_k\bar{\bar{\rho}}_k\hat{\ddot{\mathbf{R}}}, \quad (15)$$

$$-\frac{1}{\Delta t}\int_{[\Delta t]_k}\rho_k\dot{\mathbf{\Omega}}\times\mathbf{r}dt=-\left(\frac{1}{\Delta t}\int_{[\Delta t]_k}\rho_k\dot{\mathbf{\Omega}}dt\right)\times\mathbf{r}=-\alpha_k\bar{\bar{\rho}}_k\hat{\dot{\mathbf{\Omega}}}\times\mathbf{r}, \quad (16)$$

$$-\frac{1}{\Delta t}\int_{[\Delta t]_k}2\rho_k\mathbf{\Omega}\times\mathbf{u}_kdt=-\frac{2}{\Delta t}\int_{[\Delta t]_k}\rho_k\mathbf{\Omega}\times\mathbf{u}_kdt=-2\alpha_k\bar{\bar{\rho}}_k\widehat{\mathbf{\Omega}\times\mathbf{u}_k}, \quad (17)$$

$$-\frac{1}{\Delta t}\int_{[\Delta t]_k}\rho_k\mathbf{\Omega}\times(\mathbf{\Omega}\times\mathbf{r})dt=-\alpha_k\bar{\bar{\rho}}_k\mathbf{\Omega}\times\widehat{(\mathbf{\Omega}\times\mathbf{r})}. \quad (18)$$

Combining Eq. (15)~(18), we obtain

$$\mathbf{F}_{\mathrm{interial},k}=-\alpha_k\bar{\bar{\rho}}_k\hat{\ddot{\mathbf{R}}}-\alpha_k\bar{\bar{\rho}}_k\hat{\dot{\mathbf{\Omega}}}\times\mathbf{r}-2\alpha_k\bar{\bar{\rho}}_k\widehat{\mathbf{\Omega}\times\mathbf{u}_k}$$
$$-\alpha_k\bar{\bar{\rho}}_k\mathbf{\Omega}\times\widehat{(\mathbf{\Omega}\times\mathbf{r})}. \quad (19)$$

One thing that should be noted here is that some variables are coupled in the last two terms in Eq. (19). Proper models or assumptions are needed to decouple the variables. If the flow is incompressible, the mass-weighted mean is the same as the phase mean, leading to $\hat{\ddot{\mathbf{R}}}=\bar{\bar{\ddot{\mathbf{R}}}}$, $\hat{\dot{\mathbf{\Omega}}}=\bar{\bar{\dot{\mathbf{\Omega}}}}$, $\widehat{\mathbf{\Omega}\times\mathbf{u}_k}=\overline{\overline{\mathbf{\Omega}\times\mathbf{u}_k}}$, and $\mathbf{\Omega}\times\widehat{(\mathbf{\Omega}\times\mathbf{r})}=\overline{\overline{\mathbf{\Omega}\times(\mathbf{\Omega}\times\mathbf{r})}}$. In this case, $\bar{\bar{\ddot{\mathbf{R}}}}$, $\bar{\bar{\dot{\mathbf{\Omega}}}}$, and $\overline{\overline{\mathbf{\Omega}\times(\mathbf{\Omega}\times\mathbf{r})}}$ can be readily calculated because $\mathbf{R}$ and $\mathbf{\Omega}$ are functions of time alone, and $\mathbf{r}$ is fixed in time. However, additional models are needed to write $\overline{\overline{\mathbf{\Omega}\times\mathbf{u}_k}}$ as $\bar{\bar{\mathbf{\Omega}}}\times\bar{\bar{\mathbf{u}}}_k$.

The time-averaged momentum equation in the moving frame is obtained by adding Eq. (19) to the existing time-averaged momentum equation in the absolute frame. The resultant equation is

$$\frac{\partial}{\partial t}\left(\alpha_k\bar{\bar{\rho}}_k\widehat{\mathbf{u}_k}\right)+\nabla\cdot\left(\alpha_k\bar{\bar{\rho}}_k\widehat{\mathbf{u}_k}\widehat{\mathbf{u}_k}\right)=-\alpha_k\nabla\bar{\bar{p}}_k+\nabla\cdot\left[\alpha_k\left(\bar{\bar{\tau}}_k+\tau_k^{\mathrm{Re}}\right)\right]+\alpha_k\bar{\bar{\rho}}_k\mathbf{g}$$
$$+(\bar{\bar{p}}_{ki}-\bar{\bar{p}}_k)\nabla\alpha_k+\widehat{\mathbf{u}_{ki}}\Gamma_k+\mathbf{M}_{ik}-\nabla\alpha_k\cdot\bar{\bar{\tau}}_{ki}$$
$$-\alpha_k\bar{\bar{\rho}}_k\hat{\ddot{\mathbf{R}}}-\alpha_k\bar{\bar{\rho}}_k\hat{\dot{\mathbf{\Omega}}}\times\mathbf{r}-2\alpha_k\bar{\bar{\rho}}_k\widehat{\mathbf{\Omega}\times\mathbf{u}_k}-\alpha_k\bar{\bar{\rho}}_k\mathbf{\Omega}\times\widehat{(\mathbf{\Omega}\times\mathbf{r})} \quad (20)$$

4. Numerical simulation

The additional force terms (Eq. (11) and (19)) have been derived in the two-fluid momentum equation. In view of numerical simulation, it is common practice to decouple the variables in the governing equations. Omitting the averaging symbols, one can write Eqs. (11) and (19) as

$$\mathbf{F}_{\text{interial},k} = -\alpha_k\rho_k\ddot{\mathbf{R}} - \alpha_k\rho_k\dot{\mathbf{\Omega}}\times\mathbf{r} - 2\alpha_k\rho_k\mathbf{\Omega}\times\mathbf{u}_k - \alpha_k\rho_k\mathbf{\Omega}\times(\mathbf{\Omega}\times\mathbf{r}). \tag{21}$$

Therefore, the followings are added to the gas and liquid momentum equations, respectively.

$$\mathbf{F}_{\text{interial},g} = -\alpha_g\rho_g\ddot{\mathbf{R}} - \alpha_g\rho_g\dot{\mathbf{\Omega}}\times\mathbf{r} - 2\alpha_g\rho_g\mathbf{\Omega}\times\mathbf{u}_g - \alpha_g\rho_g\mathbf{\Omega}\times(\mathbf{\Omega}\times\mathbf{r}), \tag{22}$$

$$\mathbf{F}_{\text{interial},l} = -\alpha_l\rho_l\ddot{\mathbf{R}} - \alpha_l\rho_l\dot{\mathbf{\Omega}}\times\mathbf{r} - 2\alpha_l\rho_l\mathbf{\Omega}\times\mathbf{u}_g - \alpha_l\rho_l\mathbf{\Omega}\times(\mathbf{\Omega}\times\mathbf{r}). \tag{23}$$

The subscripts g and l stand for the gas and liquid phases, respectively. The interfacial jump conditions for mass, momentum, and internal energy are frame indifferent; their forms remain formally unchanged under a change of frame. Numerical simulations were made of air-water two-phase flows in this study. The flow is assumed to be incompressible and adiabatic. The two-fluid equations for mass and momentum are simplified as follows:

$$\frac{\partial\alpha_g}{\partial t} + \nabla\cdot(\alpha_g\mathbf{u}_g) = 0, \tag{24}$$

$$\frac{\partial\alpha_l}{\partial t} + \nabla\cdot(\alpha_l\mathbf{u}_l) = 0, \tag{25}$$

$$\frac{\partial}{\partial t}\left(\alpha_g\rho_g\mathbf{u}_g\right) + \nabla\cdot\left(\alpha_g\rho_g\mathbf{u}_g\mathbf{u}_g\right) = -\alpha_g\nabla p + \nabla\cdot[\alpha_g\boldsymbol{\tau}_g] + \alpha_g\rho_g\mathbf{g} + \mathbf{M}_{ig} + \mathbf{F}_{\text{inertial},g}, \tag{26}$$

$$\frac{\partial}{\partial t}(\alpha_l\rho_l\mathbf{u}_l) + \nabla\cdot(\alpha_l\rho_l\mathbf{u}_l\mathbf{u}_l) = -\alpha_l\nabla p + \nabla\cdot[\alpha_l\boldsymbol{\tau}_l] + \alpha_l\rho_l\mathbf{g} + \mathbf{M}_{il} + \mathbf{F}_{\text{inertial},l}. \tag{27}$$

The addition force terms, Eqs. (22) and (23), were implement by the help of user-defined function in ANSYS FULENT. In general, the interfacial momentum transfer between two phases is assumed to be given by the sum of the interfacial drag, lift, virtual mass, turbulent dispersion, and wall lubrication. In this study, however, the only interfacial drag [20] was considered to minimize the interfacial momentum transfer effect. The interfacial drag acting on the gas phase is given by

$$\mathbf{M}_{ig} = \frac{1}{8}\rho_l C_D a_i|\mathbf{u}_g - \mathbf{u}_l|(\mathbf{u}_g - \mathbf{u}_l), \tag{28}$$

$$C_D = \begin{cases} 24\left(1+0.15\text{Re}_b^{0.687}\right)/\text{Re} & \text{Re}\le 1000 \\ 0.44 & \text{Re} > 1000 \end{cases}, \tag{29}$$

$$\text{Re}_b = \frac{\rho_l|\mathbf{u}_g - \mathbf{u}_l|d_b}{\mu_l}, \tag{30}$$

where d_b is the bubble diameter (set to 1 mm) and $a_i = 6\alpha_g/d_b$ is the interfacial area density. For the free surface, a_i is usually small such that the simulation is unstable. As a solution, a_i is often determined based on the bubble diameter. The interfacial drag just has to be high enough to make simulation stable. Fortunately, the interfacial drag plays a minor role in predicting the free position. The gravity and acceleration acting the liquid are important. The

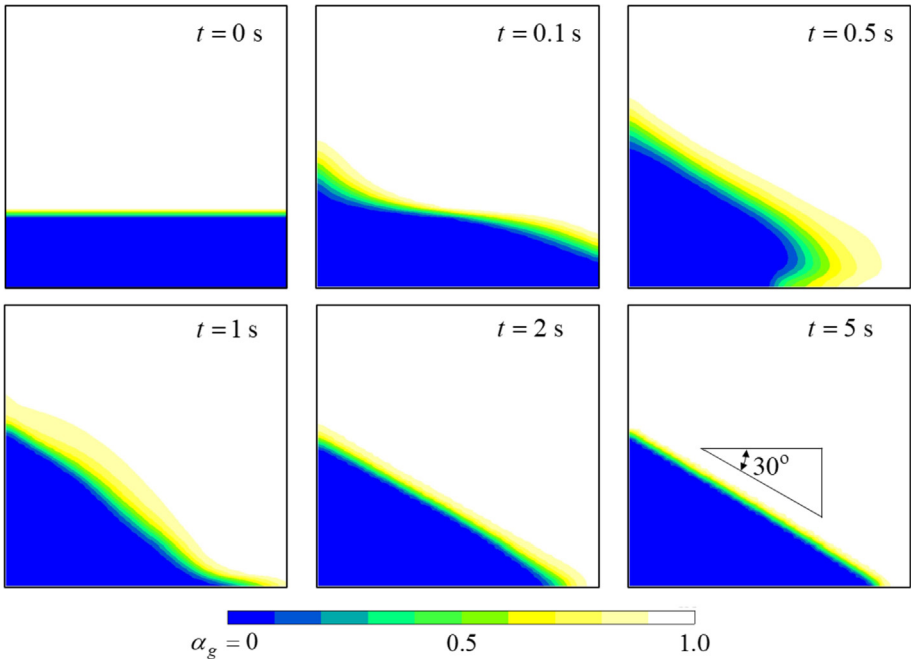

Fig. 2. Simulation result for the square tank with a horizontal acceleration of 5.6638 m^2/s.

interfacial drag acting on the liquid phase is given by $\mathbf{M}_{il} = -\mathbf{M}_{ig}$.

We will show six different simulation results to demonstrate the applicability of the two-fluid model to two-phase flows in moving systems. All simulations were performed for air-water fluids at a room temperature (25 °C) under atmospheric pressure.

4.1. Constant horizontal acceleration

The first case is a square tank subjected to a constant horizontal acceleration. This simulation is to validate the linear acceleration term ($-\alpha_k\rho_k\ddot{\mathbf{R}}$) in Eq. (21). A tank of 25 cm per side is initially filled up to 6.25 cm. The tank is accelerated as follows:

$$\ddot{\mathbf{R}} = \begin{cases} 0, & t<0 \\ 5.6638\,\mathbf{i}\ \mathrm{m}^2/\mathrm{s}, & t\geq 0 \end{cases}. \tag{31}$$

The simulation domain consists of 50 × 50 cells. Fig. 2 shows the void fraction distributions when the tank accelerates at 5.6638 m^2/s in the right direction. At the steady state (t = 5 s), the interface angle coincides with the theoretical value of $\tan^{-1}$ (5.6638/9.81) = 30°.

4.2. Horizontal oscillation

The second case is a square tank excited by forced horizontal oscillation. The objective is to validate the linear acceleration term ($-\alpha_k\rho_k\ddot{\mathbf{R}}$). The tank size is 0.9 m, and the initial water depth is 0.6 m (Fig. 3). Slip conditions is applied to the walls for comparison with an existing numerical result based on the boundary element method [21]. The tank position in the absolute frame is given by

$$R_X = A_X \sin(\omega t), \tag{32}$$

where A_X is the excitation amplitude of 0.002 m, and ω is the angular velocity of 5.5 rad/s near the natural frequency of the free surface, i.e., resonance frequency. These conditions are the same as those used in Ref. [21]. Use of two-fluid equations implies that one would accept moderate results with less grids. In addition, it is well known that the grid convergence is not always guaranteed in the two-fluid equation system. A finer grid may permit the appearance of spurious waves unless the two-fluid equations are properly regulated [22]. In these regards, it is not easy to determine the best grid numbers. Fig. 4 shows the time histories of the free surface height on the right vertical wall with four different grid sizes. The free surface was estimated by

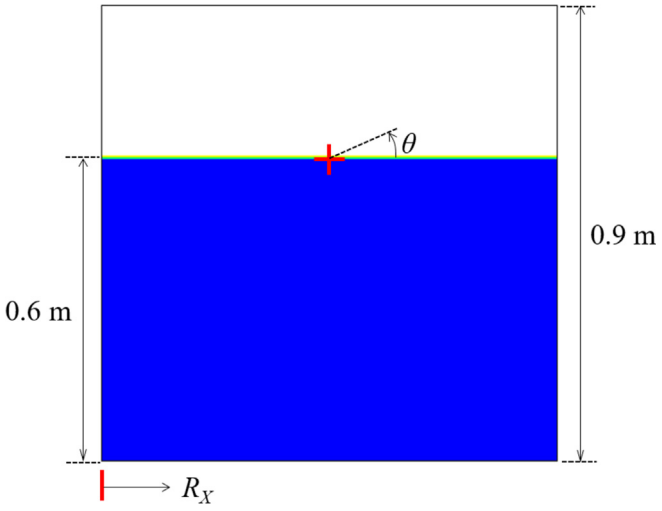

Fig. 3. Square tank partially filled with water (Nakayama's condition).

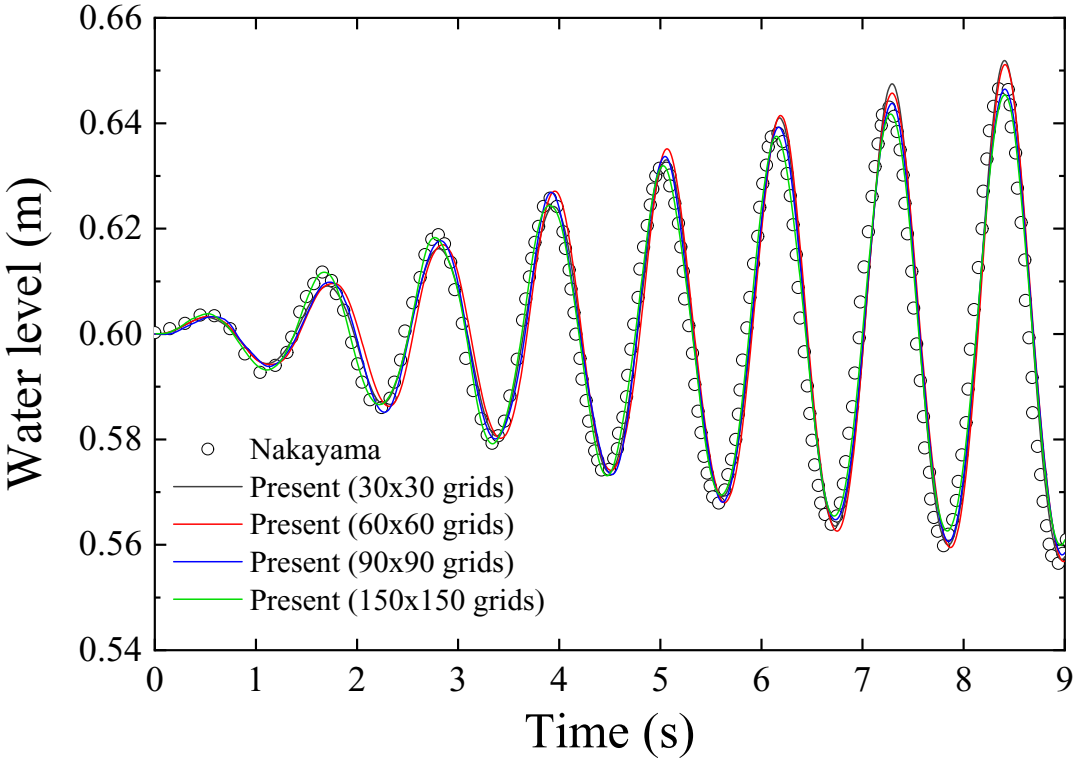

Fig. 4. Height of the free surface on the right vertical wall of Nakayama's tank with horizontal oscillation (A_X = 0.002 m, ω = 5.5 rad/s).

$$\text{water level} = \int_0^H \alpha_l dy. \tag{33}$$

where $H = 0.9$ m is the vertical dimension of the tank. As the grid size decreases, the high peaks get close to existing numerical predictions while the low peak is under-predicted. The grid size does not have a large effect on the prediction, by and large. The amplitude of the free surface oscillation increases with time even though the excitation amplitude is very small.

4.3. Rotational oscillation

The third case is the same as the second case, except the oscillation type. Initially, the water is 2/3 full of the tank and the tank is tilted $\theta_m = 0.8^o$. The tilt axis is indicated by symbol '+' in Fig. 3. The tank is assumed to be subjected to

$$\theta = \theta_m \cos(\omega t), \tag{34}$$

where ω is the angular velocity of 5.5 rad/s. In this condition, the centrifugal, Euler, and Coriolis effects are negligible as the maximum rotation speed ($\theta_m \omega^2$) is small. This case is to validate the effect of time-dependent gravity direction on the water motion. Since the tank is slightly tilted at $t = 0$, a fine grid was used to define the initial position of the free surface.

Fig. 5 shows the time history of the free surface height on the right vertical wall with 150 × 150 grids. The present two-fluid model is as accurate as the one-fluid model [21]. In general, the number of equations are larger in the two-fluid equation set than the one-fluid equation set. Therefore, for flows with large interfaces, the two-fluid model may be less efficient than the one-fluid model. The two-fluid model is beneficial to the situation in which there are numerous small interfaces in the large flow domain.

4.4. Constant rotation

The fourth case is to test the centrifugal force ($-2\alpha_k \rho_k \mathbf{\Omega} \times \mathbf{u}_k$) and the Coriolis force ($-\alpha_k \rho_k \mathbf{\Omega} \times (\mathbf{\Omega} \times \mathbf{r})$). A square tank of 0.1 m per side is subjected to a counter-clockwise rotation. No-slip conditions are imposed on the wall. The gravity effect is not considered in this case, and the rotation speed is $\omega = 2\pi$ rad/s. The simulation domain consists of 50 × 50 grids. Fig. 6 shows the void fraction distributions inside the tank. Initially, the center region of the tank is filled with water. The initial water region has a square shape with a side length of 0.06 m. At the early stage ($t = 0.1$ s), due to the centrifugal effect, the water flows in the radial and outward direction when viewed in the tank. At the same time, due to the Coriolis effect, the water flows rightward in the tank. These two effects make the water collide with the right vertical wall at $t = 0.2$ s. After five rotations ($t = 5.0$), the steady state water region is in good agreement with the theoretical region. This result implies that the centrifugal and Coriolis terms works well.

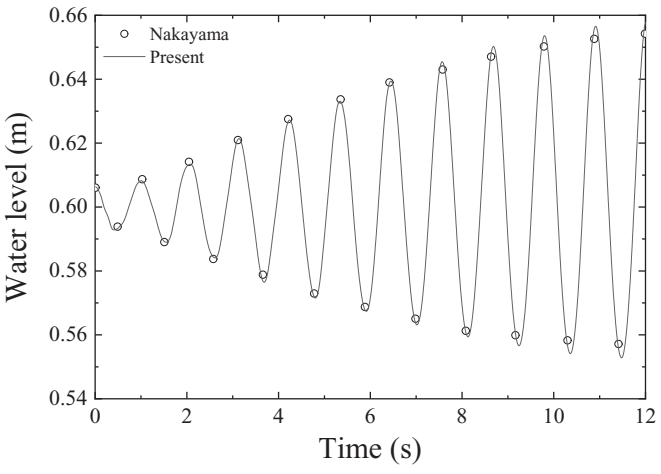

Fig. 5. Height of the free surface on the right vertical wall of Nakayama's tank with rotational pitching oscillation ($\theta_m = 0.8°$, $\omega = 5.5$ rad/s).

4.5. Complex motion with rotation

The next case is a square tank with a complex motion. The tank with a side length of 0.1 m is partially filled with water up to 0.02 m. The tank is rolling clockwise on its side shown in Fig. 7. No-slip conditions are applied to the walls. Gravity is considered in this case. The conditions are the same as those in Ref. [6], except for the initial water height. In this situation, the change of gravity direction depending on the tank orientation is also important. The complex motion of the tank may be decomposed into translational and rotational components. However, for the tank rolling on the ground, the pure translation of the tank does not exist as the rotation results in the translation. Therefore, the three rotational effects as well as the tank orientation effects are important in this study. The simulation domain consists of 50 × 50 cells. Fig. 7 shows the void fraction distributions in the tank. The water sloshing behavior is qualitatively correct.

4.6. Complex motion with both vertical and rotation oscillations

The final case is regarding the water sloshing in the oscillating manometer tank. Fig. 8 shows the initial water in the manometer. The water is half full in the manometer. The top is open to the atmosphere and a pressure boundary condition is imposed there. No-slip conditions are imposed on the other walls. The square mesh size is 0.008 m. We first consider a rotational oscillation. The oscillating axis is indicated by the symbol '+' in Fig. 8. The inclined angle θ is given by

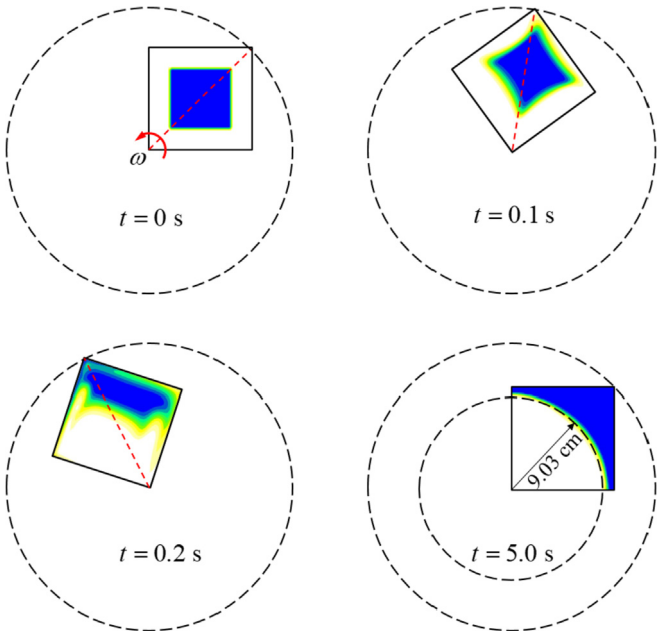

Fig. 6. Simulation result for the rotating square tank ($\omega = 2\pi$ rad/s).

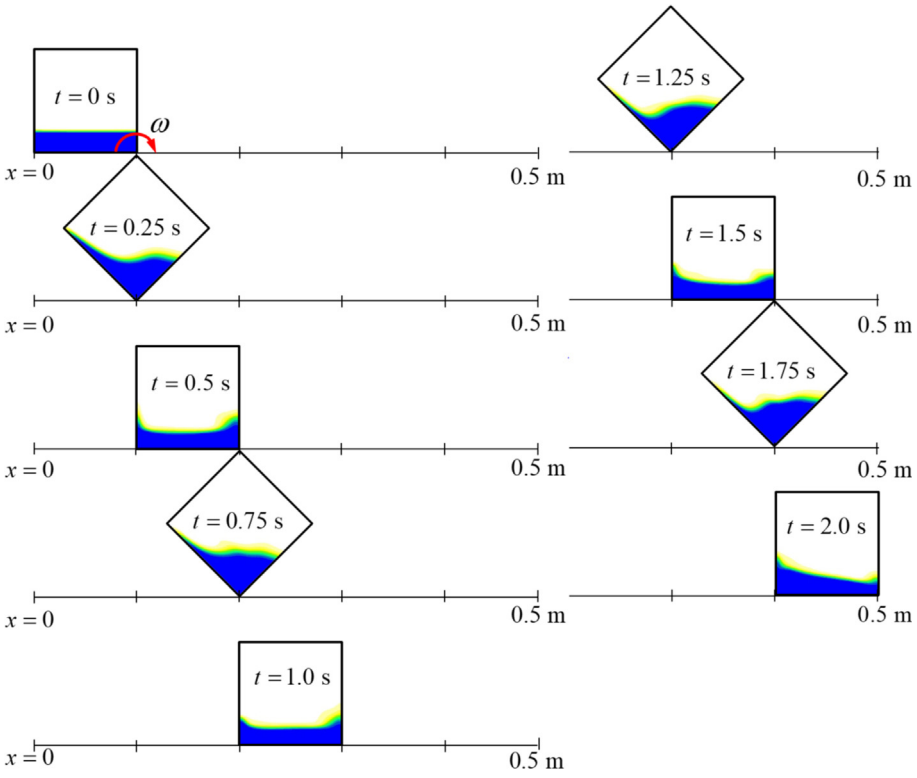

Fig. 7. Simulation result for the rolling square tank with $\omega = \pi$ rad/s.

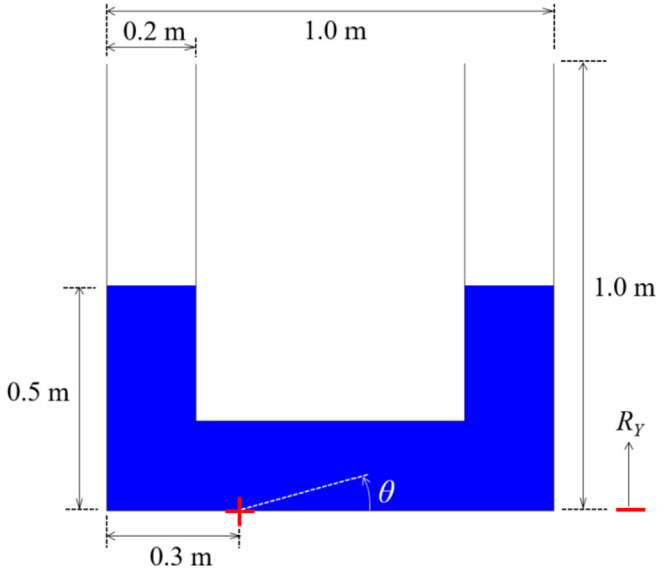

Fig. 8. Manometer partially filled with water.

$$\theta = \theta_m \sin(\omega t), \tag{35}$$

where $\theta_m = 10^o$ is the rotational oscillation amplitude, and $T = 2\pi/\omega = 2$ s is the oscillation period. Fig. 9 shows the result during one periodic cycle. The free surface is observed due to the mild oscillation.

We now add a vertical oscillation to the previous case; the manometer is oscillating vertically as well as rotationally at the same time. The vertical position of the manometer is given by

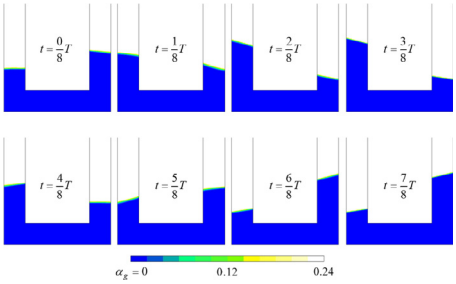

Fig. 9. Simulation result for the manometer with rotational oscillation ($\theta_m = 10^\circ$, $T = 2$ s).

$$R_Y = A_Y \sin(\omega t), \tag{36}$$

where $A_Y = 0.6$ m is the vertical oscillation amplitude, and $T = 2\pi/\omega = 2$ s is the oscillation period. In this situation, all terms in Eq. (21) are active. Fig. 10 shows the result. The combined oscillation leads to a complicated flow pattern such that some air is sucked into the lower horizontal part of the tank. As a result, the instantaneous void fraction is predicted to increase up to about 0.25 in the water region. This situation may be encountered in the downcomer of an ocean reactor in case of loss-of-coolant accident. The gas suck into the nuclear fuel assembly may influence the heat transfer between the fuel and the coolant (see Fig. 10).

The two-fluid model consists of various modeling terms such as interfacial momentum transfer, bubble agitation effect, and two-phase turbulence. As mentioned earlier, we just included the interfacial drag force among other force terms. Thus, it can be said that the result shown in Fig. 10 may be somewhat qualitative. At this time, accurate interfacial momentum transfer models under oscillating conditions have been reported yet.

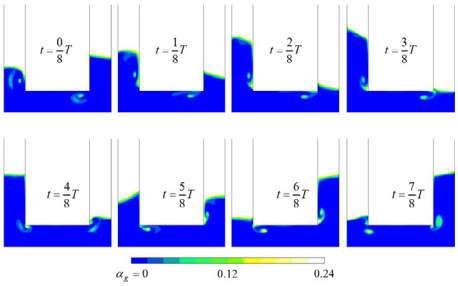

Fig. 10. Simulation result for the manometer with both rotational oscillation and vertical oscillation ($\theta_m = 10°$, $A_Y = 0.6$ m, $T = 2$ s).

We proposed the two-fluid equations in the moving systems. For this approach to be used for nuclear system analysis, closure models should be improved considering phase change under oscillating conditions even though the forms of mass and energy two-fluid equations are the same as those in the absolute frame of reference. This model improvement will be studied in the future.

5. Conclusions

Multi-dimensional two-fluid equations have been systematically derived for two-phase flows in a moving system. The averaged conservation equations for thermodynamic properties such as mass, internal energy, and enthalpy remain formally unchanged under a change of frame. The same is true for the interfacial jump conditions. However, the two-fluid momentum equation is not frame indifferent. As for volume-averaging, Eq. (11) is be added to the existing form of the volume-averaged momentum equation:

$$\mathbf{F}_{\text{interial},k} = -\alpha_k\overline{\overline{\rho}}_k\ddot{\mathbf{R}} - \alpha_k\overline{\overline{\rho}}_k\dot{\boldsymbol{\Omega}}\times\widehat{\mathbf{r}_k} - 2\alpha_k\overline{\overline{\rho}}_k\boldsymbol{\Omega}\times\widehat{\mathbf{u}_k} - \alpha_k\overline{\overline{\rho}}_k\boldsymbol{\Omega}\times\left(\boldsymbol{\Omega}\times\widehat{\mathbf{r}_k}\right). \tag{37}$$

As for time-averaging, Eq. (19) is added to the existing form of the time-averaged momentum equation:

$$\mathbf{F}_{\text{interial},k} = -\alpha_k\overline{\overline{\rho}}_k\widehat{\ddot{\mathbf{R}}} - \alpha_k\overline{\overline{\rho}}_k\widehat{\dot{\boldsymbol{\Omega}}}\times\mathbf{r} - 2\alpha_k\overline{\overline{\rho}}_k\widehat{\boldsymbol{\Omega}\times\mathbf{u}_k} - \alpha_k\overline{\overline{\rho}}_k\boldsymbol{\Omega}\times\widehat{(\boldsymbol{\Omega}\times\mathbf{r})}. \tag{38}$$

Numerical simulations were performed for six different cases using Eq. (21):

$$\mathbf{F}_{\text{interial},k} = -\alpha_k\rho_k\ddot{\mathbf{R}} - \alpha_k\rho_k\dot{\boldsymbol{\Omega}}\times\mathbf{r} - 2\alpha_k\rho_k\boldsymbol{\Omega}\times\mathbf{u}_k - \alpha_k\rho_k\boldsymbol{\Omega}\times(\boldsymbol{\Omega}\times\mathbf{r}). \tag{39}$$

For flows with free surfaces, the two-fluid approach was as accurate as the one-fluid approach. The results were in excellent agreement with theoretical/existing results. For bubbly flows in a large domain, the result demonstrated the applicability of the two-fluid approach to two-phase flows with both large and small interfaces in a large moving systems. It is expected that the multi-dimensional two-fluid equations contribute to safety/design analysis for ocean nuclear reactors.

Acknowledgements

This work was supported by the National Research Foundation of Korea (NRF) funded by Ministry of Science and ICT (Grant No. NRF-2016M2B2A9A02944972). This work was supported by the National Research Foundation of Korea (NRF) funded by Ministry of Science and ICT (Grant No. NRF- 2017M2A8A4016738).

Appendix A. Phase mean and mass-weighted mean

Let c_k be an arbitrary variable for phase k. The phase mean ($\overline{\overline{c}}_k$) and the mass-weighted mean ($\widehat{c_k}$) are defined in Table 1. The same average symbols are used for both volume-averaging and time-averaging.

Table 1
Definition of the phase mean and mass-weighted mean.

	Phase mean	Mass-weighted mean
Volume average	$\overline{\overline{c}}_k = \frac{1}{V_k}\int_{V_k} c_k dV$	$\widehat{c_k} = \int_{V_k}\rho_k c_k dV / \int_{V_k}\rho_k dV = \overline{\overline{\rho_k c_k}}/\overline{\overline{\rho}}_k$
Time average	$\overline{\overline{c}}_k = \frac{1}{[\Delta t]_k}\int_{[\Delta t]_k} c_k dt$	$\widehat{c_k} = \int_{[\Delta t]_k}\rho_k c_k dt / \int_{[\Delta t]_k}\rho_k dt = \overline{\overline{\rho_k c_k}}/\overline{\overline{\rho}}_k$

The following relations are used to formulate the averaged conservation equations.

$$\frac{1}{V}\int_{V_k}\rho_k c_k dV = \frac{V_k}{V}\frac{1}{V_k}\int_{V_k}\rho_k c_k dV = \alpha_k\overline{\overline{\rho}}_k\widehat{c_k}, \tag{A1}$$

$$\frac{1}{\Delta t}\int_{[\Delta t]_k}\rho_k c_k dt = \frac{[\Delta t]_k}{\Delta t}\frac{1}{[\Delta t]_k}\int_{[\Delta t]_k}\rho_k c_k dt = \alpha_k\overline{\overline{\rho}}_k\widehat{c_k}. \tag{A2}$$

For an incompressible flow, the two mean values are equal ($\widehat{c_k} = \overline{\overline{c}}_k$).

References

[1] J. Buongiorno, J. Jurewicz, M. Golay, N. Todreas, The offshore floating nuclear plant concept, Nucl. Technol. 194 (2016) 1–14.
[2] K. Lee, K.-H. Lee, J.I. Lee, Y.H. Jeong, P.-S. Lee, A new design concept for offshore nuclear power plants with enhanced safety features, Nucl. Eng. Des. 254 (2013) 129–141.
[3] K. Shirvan, R. Ballinger, J. Buongiorno, C. Forsberg, M. Kazimi, N. Todreas, Technology selection for offshore underwater small modular reactors, Nucl. Eng. Technol. 48 (2016) 1303–1314.
[4] Y.G. Chen, K. Djidjeli, W.G. Price, Numerical simulation of liquid sloshing phenomena in partially filled containers, Comput. Fluids 38 (2009) 830–842.
[5] W. Chung-Yueh, T. Jyh-tong, H.G, P.G, Numerical simulation of sloshing motion inside a two dimensional rectangular tank by level set method, Int. J. Numer. Methods Heat Fluid Flow 21 (2011) 5–31.
[6] R. Elahi, M. Passandideh-Fard, A. Javanshir, Simulation of liquid sloshing in 2d containers using the volume of fluid method, Ocean. Eng. 96 (2015) 226–244.
[7] D. Liu, P. Lin, A numerical study of three-dimensional liquid sloshing in tanks, J. Comput. Phys. 227 (2008) 3921–3939.
[8] L. Lu, S.-c. Jiang, M. Zhao, G.-q. Tang, Two-dimensional viscous numerical simulation of liquid sloshing in rectangular tank with/without baffles and comparison with potential flow solutions, Ocean. Eng. 108 (2015) 662–677.
[9] A.E.P. Veldman, J. Gerrits, R. Luppes, J.A. Helder, J.P.B. Vreeburg, The numerical simulation of liquid sloshing on board spacecraft, J. Comput. Phys. 224 (2007)

82–99.
[10] D.A. Drew, Mathematical modeling of two-phase flow, Annu. Rev. Fluid Mech. 15 (1983) 261–291.
[11] M. Ishii, Thermo-Fluid Dynamic Theory of Two-phase Flow, Eyrolles, Paris, France, 1975.
[12] D.Z. Zhang, A. Prosperetti, Ensemble phase-averaged equations for bubbly flows, Phys. Fluids 6 (1994) 2956–2970.
[13] J. Hao, W. Chen, Z. Chen, The development of natural circulation operation support program for ship nuclear power machinery, Ann. Nucl. Energy 50 (2012) 199–205.
[14] I. Ishida, T. Kusunoki, H. Murata, T. Yokomura, M. Kobayashi, H. Nariai, Thermal-hydraulic behavior of a marine reactor during oscillations, Nucl. Eng. Des. 120 (1990) 213–225.
[15] G.L. Mesina, D.L. Aumiller, F.X. Buschman, M.R. Kyle, Modeling moving systems with relap5-3d, Nucl. Sci. Eng. 182 (2016) 83–95.
[16] B.H. Yan, L. Yu, Theoretical Research for natural circulation operational characteristic of ship nuclear machinery under ocean conditions, Ann. Nucl. Energy 36 (2009) 733–741.
[17] B.H. Yan, L. Yu, The development and validation of a thermal hydraulic code in rolling motion, Ann. Nucl. Energy 38 (2011) 1728–1736.
[18] B.H. Yan, L. Yu, The experimental and theoretical analysis of a natural circulation system in rolling motion, Prog. Nucl. Energy 54 (2012) 123–131.
[19] M. Ishii, T. Hibiki, Thermo-Fluid Dynamics of Two-phase Flow, 2nd, Springer, New York, USA, 2011.
[20] L. Schiller, Z. Naumann, A drag coefficient correlation, Z. Ver. Deutsch. Ing. 77 (1935) 318–320.
[21] T. Nakayama, K. Washizu, The boundary element method applied to the analysis of two-dimensional nonlinear sloshing problems, Int. J. Numer. Methods Eng. 17 (1981) 1631–1646.
[22] A. Prosperetti, Averaged equations for multiphase flow, in: A. Prosperetti (Ed.), Computational Methods for Multiphase Flow, Cambridge University Press, Yew York, USA, 2007, pp. 237–281.